A Digitally Controlled MEMS Gyroscope With Unconstrained Sigma-Delta Force-Feedback Architecture

J. Raman[1], *E. Cretu*[2], *P. Rombouts*[1], *and L. Weyten*[1]
[1]Ghent University (UGent-ELIS-CAS), Ghent, BELGIUM
[2]Melexis N.V., Tessenderlo, BELGIUM

ABSTRACT

In this paper we describe the system architecture and prototype measurements of a MEMS gyroscope with a resolution of $0.055\,°/s/\sqrt{\mathrm{Hz}}$. Two innovations are presented. The first is the complete migration of control and demodulation tasks to the digital domain. For this purpose, interfacing circuits based on $\Sigma\Delta$ techniques are introduced for both primary and secondary mode. The advantage is that complex analog electronics for tracking the resonant frequency, stabilizing the amplitude of the primary mode oscillation and phase-sensitive demodulation can be replaced by their digital counterpart. A second innovation relates to the $\Sigma\Delta$ force-feedback loop. In previously reported structures a compensation filter is introduced for stabilizing the loop [1–3]. Unfortunately, the compensation filter introduces extra poles and influences the noise-shaping characteristic, which makes the loop difficult to design and optimize. We demonstrate the possibility of obtaining a stable $\Sigma\Delta$ force-feedback loop *without* an explicit compensation filter.

1. INTRODUCTION

For the automotive industry, the rise of MEMS technology opened the way toward low-cost inertial sensors for various safety and comfort systems. Perhaps initially the focus has been on accelerometers. However, applications ranging from rollover detection to inertial navigation also vitalized a growing interest in MEMS gyroscopes. It is to be expected that future market requirements will emphasize on higher resolution and better long-term behavior. Unfortunately, the development of high-performance micromachined gyroscopes is hindered by a series of technology-related imperfections of the mechanical structure. These imperfections manifest themselves for instance in the existence of error components largely exceeding the signal to be measured (quadrature error). This imposes difficult requirements with respect to the dynamic range of readout and interface circuits. Also, the fact that mechanical parameters are unknown (due to fabrication variations, fluctuations with temperature and aging) poses serious challenges.

These problems promote the use of closed-loop solutions. First, the parameters of the primary mode oscillation are stabilized by feedback control. This solves the strong dependence on the resonant frequency and quality factor of the primary mode. Second, closed-loop readout of the sense mode also brings distinct advantages. In closed-loop, the Coriolis force is measured by comparing with a (temperature-independent) feedback force. In practice, a much lower sensitivity to variations in mechanical parameters of the secondary mode can be obtained.

Another advantage of applying force-feedback to the secondary mode is that the dynamic range of the readout setup can be significantly improved. Indeed, by increasing the maximum attainable feedback force, larger input forces can be measured without saturating the readout and interface circuits (because these circuits only process the error signal). This increased dynamic range is important for dealing with the large parasitic forces causing the quadrature error.

The challenge of detecting the weak Coriolis coupling from primary to secondary mode in the presence of strong parasitic couplings requires a significant amount of signal processing. In this paper, interfacing circuits based on $\Sigma\Delta$ techniques are inserted to allow a quick transition to and from the digital domain. While the advantages of a $\Sigma\Delta$ force-feedback loop for readout of the secondary mode have already been recognized in the literature [1, 3], we show that $\Sigma\Delta$-techniques can also be used for operating the primary mode in closed loop. This strategy allows the migration of most control tasks completely to the digital domain: tracking of the resonant frequency, amplitude stabilization of the primary mode and phase-sensitive demodulation. The technique also opens up new possibilities toward advanced model-based signal processing to increase the overall performance of the system.

2. SYSTEM-LEVEL OVERVIEW

A system-level representation of the gyroscope is shown in fig. 1. The overall functioning is as follows. From a digital quadrature oscillator (DCO), a sinusoidal signal is derived which defines the wanted driving force. Both the frequency and the amplitude of this driving force can be controlled. The multi-bit force signal is converted to an oversampled one-bit signal with a digital $\Sigma\Delta$-modulator. This one-bit signal is further used for actuation. Depending on the binary value, an electrostatic force F_{el} is applied in either the positive or the negative x-direction (driven mode): $F_{x,drive} = \pm F_{el}$. This is accomplished by applying a fixed voltage to a comb-like actuator, which results in force pulses with constant magnitude, independent of the position of the proof mass in the x-direction. As a result, the actuation approach realizes an inherent digital-to-force conversion with good linearity.

The mechanical structure reacts to this continuous sequence of force pulses (arriving at a high rate) in a frequency-selective way. Because of the resonant nature of the mechanical transfer

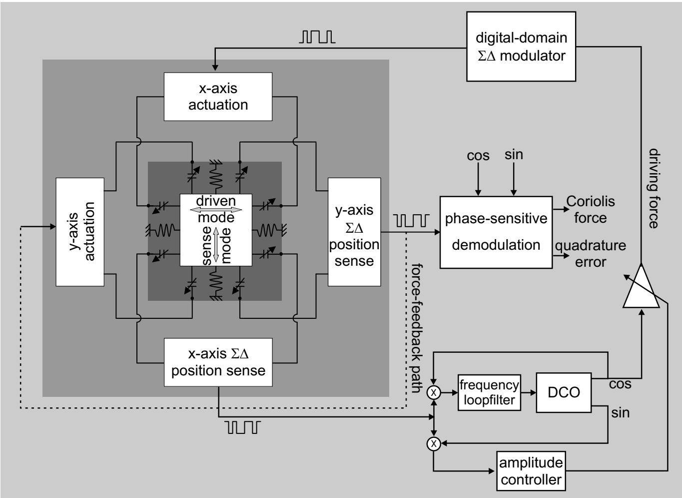

Fig. 1. System-level overview: mechanical sensor (dark grey), interface electronics (medium grey) and digital functions (light grey).

of the primary mode, signals close to the resonant frequency are amplified (resulting in movement), while out-of-band frequencies are filtered out (and hence induce little motion). To make full use of this frequency-selective mechanism, the noise shaping of the digital ΣΔ-modulator is optimized to push quantization noise as much as possible away from the frequency-range-of-interest, which is basically only a small band around the resonant frequency.

In order to further close the loop, the displacement in the x-direction is measured by a capacitive readout circuit and converted to the digital domain through an electrical ΣΔ modulator. The driving frequency is digitally adapted up to the point where the displacement is $90\,^\circ$ out of phase with the driving force. Also, the driving force amplitude is controlled for stabilizing the amplitude of the primary mode oscillation, resulting in a complete closed-loop control of the driven mode. For readout of the secondary-mode displacement, a ΣΔ force-feedback loop is set up (detailed in the next section). The resulting output is demodulated digitally to separate the Coriolis signal from the quadrature error.

3. UNCONSTRAINED ΣΔ FORCE-FEEDBACK ARCHITECTURE

We already pointed out that using force-feedback is interesting for making the readout of the secondary mode less susceptible to variations in mechanical parameters and to increase the dynamic range. Among the possible force-feedback solutions, techniques based on single-bit ΣΔ-modulation attract much attention because of their good linearity and inherent analog-to-digital conversion. However the additional noise due to quantization needs to be considered. In order not to impose a cost in terms of resolution, quantization noise should be below the electronic noise of the readout front-end in the frequency-range-of-interest. Therefore, the transfer from quatization noise to the output of the ΣΔ force-feedback loop — commonly called the noise transfer function (NTF) — needs to obtain a desired shape.

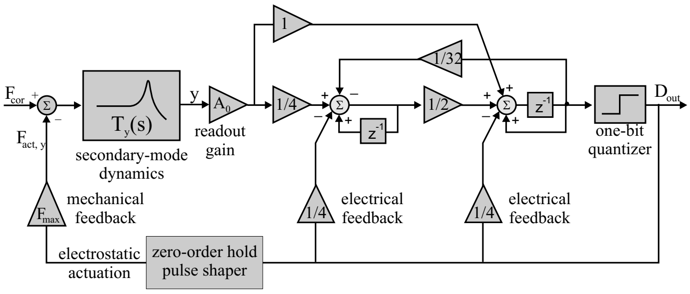

Fig. 2. Implemented unconstrained ΣΔ force-feedback architecture.

For purely electrical ΣΔ modulators, a common design strategy is to concentrate first on deriving a good NTF (one that optimizes the performance/stability trade-off), and only after this to make a choice among different architectures that can realize this NTF. For ΣΔ force-feedback loops, this design approach is hindered by the fact that the mechanical transfer is of second order and has no direct access to its intermediate (speed) node. Therefore, for ΣΔ force-feedback loops, this decoupled design method has until now not been followed in the literature. Instead, a control-theory based design cycle is used where an extra compensation filter (often a simple FIR filter $1 - \alpha z^{-1}$, see [3]) is introduced for stabilizing the loop. Unfortunately, this controller introduces extra poles in the loop (for FIR filters at $z = 0$), increasing the actual order of the NTF. To the authors' knowledge, all ΣΔ force-feedback architectures presented until now have an order-increasing controller which introduces implicit constraints on the realizable NTF.

In this paper, we present a new architecture for a ΣΔ force-feedback loop (fig. 2). Next to the shaping from the mechanical transfer, an electrical resonator is added to the loop to provide a notch in the NTF at the operating frequency of the gyroscope. Similar to [3], the electrical resonator is built by applying local feedback to a delaying and non-delaying integrator. In order to understand the rationale behind the proposed solution, we return again to the main difficulty: the fact that we are not able to couple to the speed node of the mechanical transfer. It is clear that we can still observe the speed indirectly, through differentiation of the readout signal (which is proportional to the displacement of the proof mass). As this differentiating path is followed by an electrical filter built from integrators, this can conceptually be replaced by a direct path bypassing the first integrator, which is the upper path in fig. 2. This extra feedforward path is in fact the main innovation of this architecture. The obtained structure contains in total two electrical forward and two electrical feedback paths. These four paths provide enough degrees-of-freedom to have complete control over the NTF poles. Since no extra controller poles are introduced, this allows to decouple the NTF design from the actual architecture, which opens the possibility to optimize the noise-shaping characteristics of the

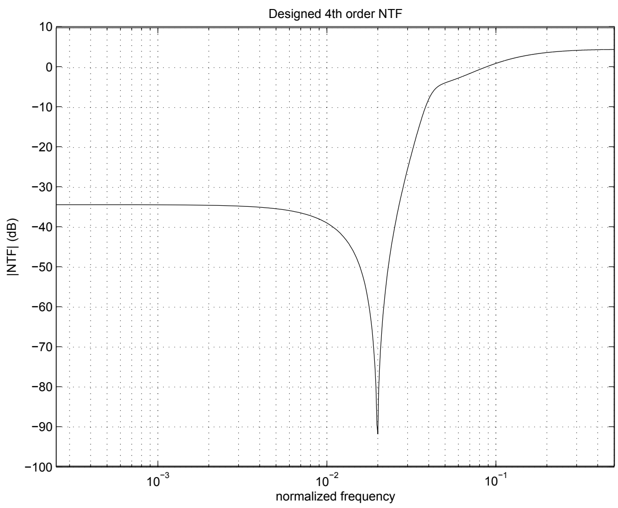

Fig. 3. Amplitude characteristic of the designed 4th order NTF. Notice that the noise shaping is optimized to push quantization noise away from the frequency-range-of-interest.

loop directly.

In order to follow this decoupled design strategy, we concentrate first on the design of the NTF itself, without reference to the architecture. To this end, we start from a pole-zero decomposition of a fourth-order NTF:

$$\mathrm{NTF}(z) = \frac{(z-z_y)(z-z_y^*)(z-z_e)(z-z_e^*)}{(z-z_1)(z-z_1^*)(z-z_2)(z-z_2^*)} \tag{1}$$

Because the NTF zeros correspond to the poles of the loop filter of the $\Sigma\Delta$ modulator, they can be directly identified. The NTF contains two complex conjugate zeros (z_y and z_y^*) due to the resonant mechanical transfer of the secondary mode:

$$z_y \approx e^{-2\pi \frac{f_y/f_s}{2Q_y}} \; e^{j2\pi f_y/f_s}$$

Here, f_s is the sample frequency, f_y the secondary mode resonant frequency and Q_y the quality factor. Typical values in this design are $f_s \approx 412$ KHz, $f_y \approx 8200$ Hz and $Q_y \approx 10$. As already pointed out, in order to improve the noise shaping in the frequency-range-of-interest, an electrical resonator is used which introduces two extra complex conjugate zeros z_e and z_e^*:

$$z_e = e^{j2\pi f_y/f_s}$$

As is usual for a higher-order $\Sigma\Delta$ systems, four NTF poles need to be introduced to obtain a stable system. In fact, the placement of these poles is related to the performance/stability trade-off of the system. After exploration of this trade-off, four NTF poles z_1, z_1^*, z_2, z_2^* have been selected, with:

$$\begin{cases} z_1 = 0.950\, e^{\pm j2\pi 0.04003} \\ z_2 = 0.593\, e^{\pm j2\pi 0.03988} \end{cases}$$

The resulting theoretical NTF has been plotted in fig. 3. Notice the steep notch in the frequency-range-of-interest.

Having established this 4th-order NTF, we can easily determine the necessary coefficients of the proposed unconstrained architecture. By using elementary scaling techniques and rounding coefficients to convenient values, the solution of fig. 2 amenable for circuit-implementation can be derived.

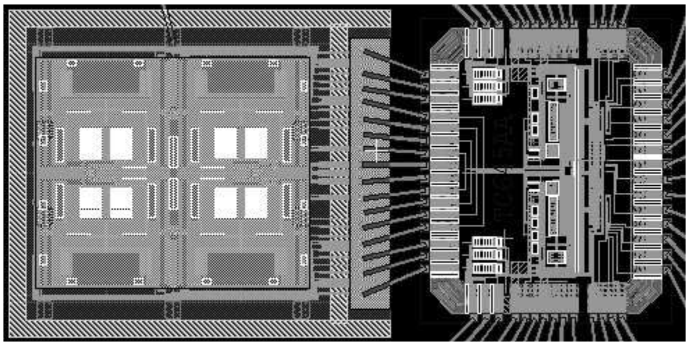

Fig. 4. Layout-view of the mechanical sensor & die photo of the interface electronics.

4. PROTOTYPE

In order to prove the feasibility of the approach, a prototype has been built (fig. 4). For the mechanical MEMS sensor, a differential topology is used to cancel acceleration-type interfering forces. A separate ASIC contains the readout and interface electronics. The mechanical and electrical die are packaged together. Rather than adding the digital processing to the electrical ASIC, we have implemented the main digital functionality in a separate FPGA. The flexibility and reprogrammability offered by the FPGA can be used to further optimize the signal processing. As can be seen on fig. 1, the proposed partitioning requires basically only four pins for interfacing between analog and digital blocks: two $\Sigma\Delta$ bit-streams that contain information on the proof mass x- and y-displacement, and two $\Sigma\Delta$ bit-streams that define the direction of actuation along the x- and the y-axis.

On the electrical side, the actual readout circuit (fig. 5) is the most critical block. For each operation mode of the mechanical sensor, two stator-connections are implemented at opposite sides. Each stator connection forms a parallel-plate capacitors with the proof mass. Displacements of the proof mass result in a differential change in these sensing capacitors. With respect to the readout circuit, also large parasitic capacitances C_p need to be taken into account. These are mainly due to bonding pads required in the two-die approach.

The basic readout principle is to actively maintain a constant potential over the readout capacitors, and detect relative changes in the charge stored on the readout capacitors. The circuit operates as follows. The potential of the proof mass is kept to ground at all the times. In order to define the voltage levels at the purely capacitive readout nodes A and B, two switched-capacitor (SC) resistors are used (encircled in fig. 5). These SC resistors are realized by periodically resetting the input capacitance C_{in} of the amplifier to V_{CMref} (during ϕ_1) and subsequently reconnecting to the readout node (during ϕ_2). During ϕ_1, when the input terminals are shorted, the amplifier is auto-zeroed (not shown on the schematic). During ϕ_2, the

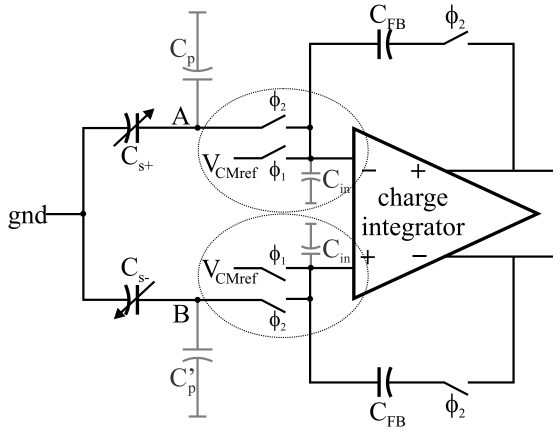

Fig. 5. Simplified schematic of the readout circuit.

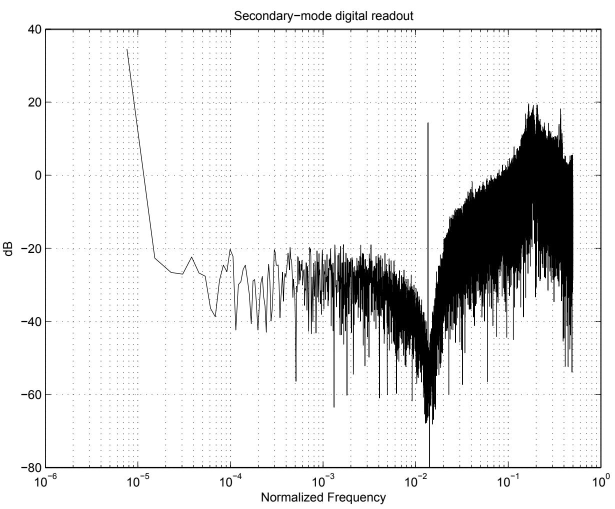

Fig. 6. Measured noise shaping of the ΣΔ force-feedback loop.

circuit is configured as a charge integrator. In this phase, the amplifier nulls the voltage difference between nodes A and B, and produces an output voltage proportional to the charge difference.

The circuit aspects of the other building blocks of the electrical ASIC are rather straightforward. For instance, the electrical resonator (as detailed in fig. 2) is implemented using standard switched-capacitor techniques. Also, the quantizer consists of a simple dynamic latch with pre-amplifier.

5. Measurements & conclusion

An interesting measurement is to observe the output of the single-bit ΣΔ force-feedback loop when no rotation rate is applied. The FFT result is displayed in fig. 6. As expected, a clear notch appears in the spectrum, which is due to the noise shaping from the mechanical and electrical resonators. Prior to the measurement of fig. 6, the sample frequency was tuned in order to match the electrical and mechanical resonant frequencies. This was needed because without tuning,

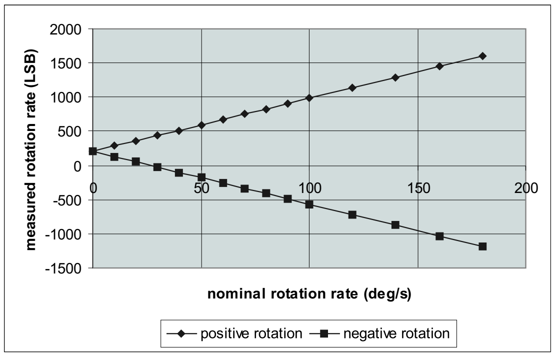

Fig. 7. Measured rotation rate as a function of applied rotation rate.

the resonant frequency of the electrical resonator deviated somewhat from its designed value. In the spectrum, also a strong spectral peak appearing at the resonant frequency can be noticed. Since the measurement is done with no rotation applied, this component is due to the quadrature error and direct electrical coupling of driving signals to the readout. Also, the existence of a large offset can be noted.

Even in the presence of large error signals like quadrature error, offsets, circuit noise etc., the ΣΔ force-feedback loop is able to operate and convert all relevant signals into the digital domain. This illustrates the high dynamic range provided by the proposed ΣΔ force-feedback loop, which forms the corner stone of the digital post-processing approach promoted in this paper. The unwanted signals can be easily removed in the digital domain.

Last but not least, in order to characterize the gyroscope as a whole, a batch of rotation rate measurements where performed (fig. 7). Because of the use of phase-sensitive demodulation, the quadrature error is largely eliminated. Still, some residual offset (approximately 213 LSB) can be noticed due to other error components. From these rotation measurements, the scale factor $S_\Omega \approx 7.73\,\mathrm{LSB}/(\,{}^\circ\!/s)$ can be extracted. In order to estimate the resolution, the standard deviation of the zero-rate was determined, which amounts to 0.73 LSB in a 3Hz bandwidth. The estimated resolutions becomes $0.055\,{}^\circ\!/s/\sqrt{\mathrm{Hz}}$.

Acknowledgement

This work is supported by the Flemish Institute for Scientific and Technological Research (IWT).

References

[1] Xuesong Jiang, Joseph I. Seegers, Michael Kraft, and Bernhard E. Boser, "A Monolithic Surface Micromachined Z-Axis Gyroscope with Digital Output", *2000 Symposium on VLSI Circuits*, Hawaii, June 2000, pp. 16–19

[2] Yufeng Dong, Michael Kraft, Carsten Gollasch and William Redman-White, "A high-performance accelerometer with a fifth-order sigma-delta modulator," *J. Micromech. Microeng.*, vol. 15, nr. 7, pp. S22-S29, July 2005.

[3] Petkov V.P. and Boser B.E., "A Fourth-Order ΣΔ Interface for Micro-machined Inertial Sensors," IEEE Journal of Solid-State Circuits, vol. 40, nr. 8, Aug. 2005, pp. 1602–1609